Pseudospectra of the Linear Navier-Stokes Evolution Operator and Instability of Plane Poiseuille and Couette Flows: (preliminary report)

Lloyd N. Trefethen*
Anne E. Trefethen
Satish C. Reddy

TR 92-1291
June 1992

Department of Computer Science
Cornell University
Ithaca, NY 14853-7501

*Supported by NSF Grant DMS-9116110.

Pseudospectra of the linear Navier-Stokes evolution operator and instability of plane Poiseuille and Couette flows: preliminary report

Lloyd N. Trefethen*
Department of Computer Science
Cornell University
Ithaca, NY 14853
lnt@cs.cornell.edu

Anne E. Trefethen
Cornell Theory Center
Cornell University
Ithaca, NY 14853
aet@tc.cornell.edu

Satish C. Reddy
Courant Institute of Mathematical Sciences
251 Mercer St.
New York, NY 10012
reddy@cims.nyu.edu

*Supported by NSF Grant DMS-9116110.

Table of Contents

Abstract

This is a rough, interim report on some new results concerning the stability of plane Poiseuille and Couette fluid flows, following upon recent work by Henningson and Reddy, Butler and Farrell, Gustavsson, and others. We emphasize that the conclusions proposed here have not yet been checked carefully and are subject to change.

Our principal results are as follows:

1. Plots of the spectra of the "full" Navier-Stokes operator for Poiseuille and Couette flows, i.e., without restriction to a wave number pair (α, β) or to even or odd modes (§§4,5).

2. Analogous plots for the pseudospectra of this operator. Comparison of the pseudospectra with the spectra gives a new interpretation of why the physics of these linear flow problems is not controlled by the location of the most unstable eigenvalue (§§4,5).

3. Demonstration that these pseudospectra predict the Butler-Farrell "optimal" transient energy growth ratios to within a factor of about 2 (§6).

4. Demonstration that about 90% of the Butler-Farrell growth can be achieved by a 3×3 linear model obtained by projecting the Navier-Stokes problem onto the space spanned by three dominant eigenmodes, for Couette flow, or four in the case of Poiseuille flow (§8).

5. Demonstration that although 1 Orr-Sommerfeld mode and 3 Squire modes suffice for the 4×4 model in the Poiseuille case, in keeping with a recent result of Gustavsson, one can do equally well with 2 modes of each kind or with 3 Orr-Sommerfeld modes and 1 Squire mode (§8).

6. Demonstration that the minimal operator perturbation required to destabilize a stable flow has norm of order R^{-2}, where R is the Reynolds number, though the distance of the least stable eigenvalue from the real axis is $O(R^{-1})$ (§7).

7. Presentation of a 2×2 model illustrating that if the linear problems described above are capable of transient energy growth of order M (e.g., $M \approx 1000$ according to Butler and Farrell), a weak and intrinsically energy-conserving nonlinear term can "bootstrap" that growth to a higher order such as M^2. This supports the view that although nonlinear terms are of course essential to the subcritical instability of fluid flows, the detailed nature of the nonlinear interactions may sometimes be relatively unimportant (§2).

8. Adaptation of this "bootstrapping" idea to the fluid flows considered earlier, particularly the 3×3 approximation for Couette flow with $R = 1000$.

1. Introduction

A change of paradigm is taking place in the field of hydrodynamic stability. The traditional paradigm is eigenvalue analysis, which can be summarized by the following sequence:

(1) Linearize about the laminar solution;

(2) Look for unstable eigenvalues of the linearized problem.

An "unstable eigenvalue" means an eigenvalue in the upper half-plane, thanks to the convention of introducing a factor $-i$ in the linearization. For planar shear flows, one of the central results of eigenvalue analysis is Squire's theorem of 1933, which asserts that in the study of the most unstable eigenvalues of a flow (i.e., eigenvalues with largest imaginary part), one may always restrict attention to 2D perturbations of the flow field [2].

For some problems (e.g. Bénard convection, Taylor-Couette flow) the predictions made by eigenvalue analysis match laboratory experiments well. These are the cases where the operator involved in the linearized model is normal (i.e., has orthogonal eigenfunctions). For other problems (e.g. plane Poiseuille, plane Couette, pipe Poiseuille flow), the predictions made by eigenvalue analysis match laboratory experiments poorly. In these problems the operator involved in the linearized model is highly non-normal, with the basis of eigenfunctions typically having a condition number that grows exponentially as a function of $R^{1/2}$ as $R \to \infty$ (R is the Reynolds number) [14,RH].

For example, eigenvalue analysis predicts a critical Reynolds number $R = 5772$ for plane Poiseuille flow, but in the laboratory, transition to turbulence is usually observed at Reynolds numbers closer to 1000. For plane Couette flow eigenvalue analysis predicts linear stability for all Reynolds numbers, but transition to turbulence is observed at Reynolds numbers as low as 350. Clearly there is a mismatch in these problems between experimental observations and predictions based on eigenvalues. This has been recognized for many years, and the explanation has usually been attributed to step (1) above. If linear analysis has failed, the reasoning goes, one must look more closely at the nonlinear terms.

Recently it has emerged, however, that the failure of eigenvalue analysis may lie principally with step (2), not step (1). Even if all of the eigenvalues of a linearized flow problem lie in the stable half-plane, solutions to that linear problem may still exhibit transient energy growth, thanks to the non-orthogonality of the eigenfunctions. If attention is restricted to 2D perturbations, in keeping with the spirit of Squire's theorem, the following transient energy growth factors are possible [4,14]:

2D Couette, $R = 1000$: 13.0

2D Poiseuille, $R = 5000$: 45.7.

However, since such transient growth is not a modal phenomenon, there is no solid reason to restrict attention to 2D perturbations. In the past two years it has been discovered that much larger transient energy growth factors are possible if one allows 3D perturbations [BF,RH,6]:

$$\text{3D Couette, } R = 1000\text{: } 1185.$$
$$\text{3D Poiseuille, } R = 5000\text{: } 4897.$$

These numbers indicate that even a linearized flow that is asymptotically stable may include a mechanism of great energy growth. Moreover, the 3D (pseudo)modes that exhibit this transient growth have the form of streamwise vortices, which have been observed for many years as a conspicuous feature in laboratory experiments.

In summary, in the past year it has begun to appear that the essential mechanism of energy growth of perturbations of plane Poiseuille and Couette flows may be linear, three-dimensional, and unrelated to eigenmodes. This emphasis on *linear but non-modal* effects is the emerging new paradigm in hydrodynamic stability.

The central people involved in these developments have been Farrell and Butler (Harvard); Henningson, Schmid, and Reddy (MIT, MIT, Courant Institute); and Gustavsson (Luleå). In particular, two key papers on 3D transient energy growth have been written recently, which we shall refer to as [BF] and [RH]:

[BF] K. M. Butler and B. F. Farrell, "Three-dimensional optimal perturbations in viscous shear flow," to appear in *Physics of Fluids*, 1992;

[RH] S. C. Reddy and D. S. Henningson, "Energy growth in viscous channel flows," submitted to *Journal of Fluid Mechanics*, 1992.

The longstanding figure in espousing the new point of view has been Brian Farrell, who in a succession of papers since 1982 has described the possibilities of non-model transient effects in fluid flows, both in meteorology and classical fluid mechanics [3,4]. The discovery of 3D transient energy growth is due to Farrell and his student Kathryn Butler in 1991, based partly on discussions with Henningson; shortly before, growth factors about 90% as large as the optimal ones had been discovered independently by Gustavsson [6]. The numbers listed above are taken from [BF].

This paper is a rough compilation of some computational results that we have obtained in recent weeks with the aid of Matlab and Fortran codes adapted from those used previously by Reddy and Henningson [RH]. These computations have led us in a number of directions, as summarized in the Abstract. We have decided to record them here in rough form before preparing one or more papers for publication that will, inevitably, cover only a subset of these issues and appear several years hence. This paper is incomplete in two respects. First, the computational results are tentative, and we will undoubtedly find that certain things have to be changed as we re-examine and extend the calculations in the upcoming months. Second, we give none of the mathematical or physical details, and few of the necessary references, but assume that the reader is already familiar with the field of hydrodynamic stability and with [BF] and [RH].

2. A 2×2 model

Subcritical transition to turbulence depends upon nonlinearity, yet we have claimed that the energy growth mechanism is essentially linear. In this section we explain what we mean by this by describing a 2×2 nonlinear model problem which, we believe, may capture some of the process of transition to turbulence. In particular this model illustrates how a linear growth mechanism of order R may be "bootstrapped" to a nonlinear growth mechanism of order R^2 or larger. We are grateful to Philip Holmes for suggesting to us the study of 2×2 models.

Let R be a large parameter and consider the matrix*

$$u_t = Au, \qquad A=\begin{pmatrix} -1 & R \\ 0 & -2 \end{pmatrix} \tag{2.1}$$

The 2×2 linear problem $u_t = Au$ has solution $u(t) = e^{tA}u(0)$, and $\|e^{tA}\|$ is the norm of the solution operator. Figure 2.1 plots this norm as a function of t for $R=1$, 10, 10^2, 10^3, and 10^4. Throughout this paper, $\|\cdot\|$ is the usual 2-norm induced by the inner product $(u,v)=\int u^* v$.

Figure 2.1 reveals the following features of the curves $\|e^{tA}\|$. The initial slope (determined by the field of values of A) is $\sim R/2$. The asymptotic slope as $t\to\infty$ (determined by the spectrum of A) is -1. In between these extremes, for finite t, there is a large hump, of height $M\sim R/4$. This corresponds to transient amplitude growth of order R, in analogy to the transient growth described in [6], [BF], and [RH].

Now let us add a nonlinear term of Hamiltonian form, i.e., one that transfers energy from the decaying modes of the linear problem to the growing mode† but does not in itself add energy. The simplest problem of this kind is

$$u_t = Au + \|u\|Bu, \qquad B=\begin{pmatrix} 0 & -1 \\ 1 & 0 \end{pmatrix} \tag{2.2}$$

for the same matrix A. The matrix B has imaginary eigenvalues, and the nonlinear term does not add energy into the system directly, as is shown by the vanishing of B from the formula

$$\begin{aligned} \frac{d\|u\|^2}{dt} = 2(u,u_t) &= 2(u,Au) + 2\|u\|(u,Bu) \\ &= 2(u,Au) = (u,(A+A^T)u). \end{aligned} \tag{2.3}$$

---

*The results would be essentially the same if we took both diagonal entries equal to -1. However, we have used the less elegant example (2.1) to make sure there is no misunderstanding that the points we are making do not depend on nondiagonalizability.

†The phrase "growing mode" here and below is careless, since the eigenmodes of this problem all decay. We are speaking of components that experience transient growth, not asymptotic.

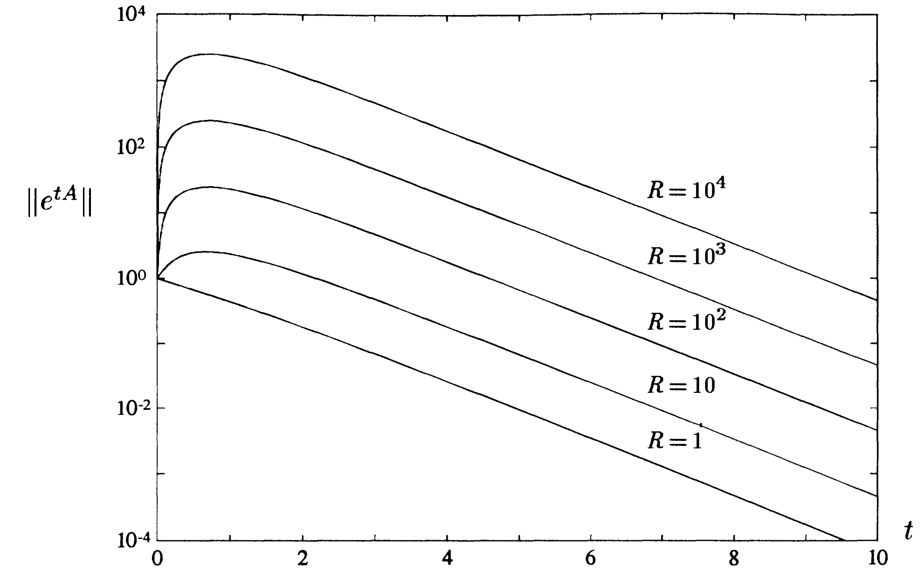

Figure 2.1. $\|e^{tA}\|$ vs. t for the linear model problem (2.1).

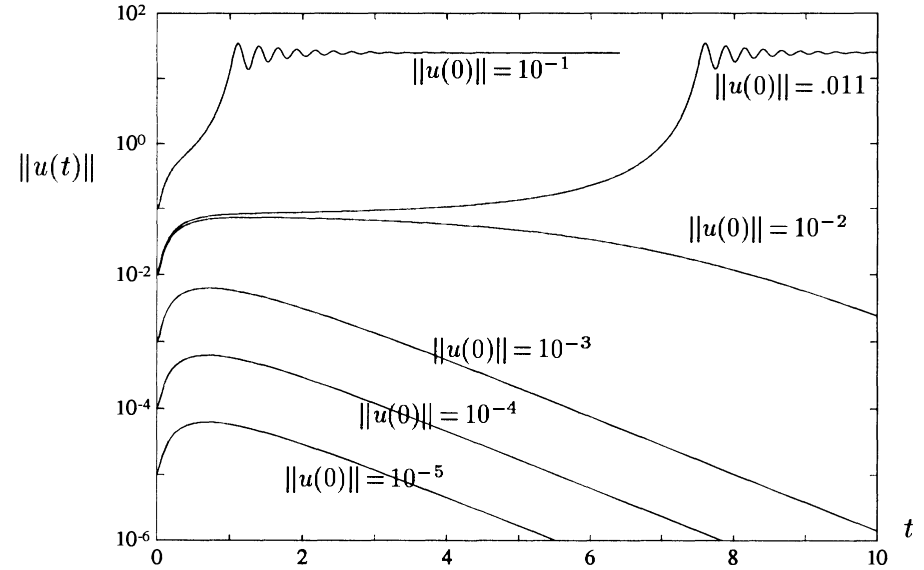

Figure 2.2. $\|u(t)\|$ vs. t for solutions to the nonlinear model problem (2.2) with $R=25$ and various initial vectors $u(0)=(0,\text{const})^T$.

R	linear growth factor M	threshold amplitude ϵ	$M^2\epsilon$
12.5	3.18	.043	.433
25	6.28	.0105	.414
50	12.5	.0026	.406
100	25.0	.00065	.406

Table 2.1. The "bootstrapping" of the linear growth factor M causes the threshold amplitude to be of order M^{-2}.

Figure 2.2 shows the effect of the nonlinear term on the solutions $u(t)$, with $R=25$. The figure shows the norms $\|u(t)\|$ for solutions starting from six different initial vectors of the form $u(0) = (0, \|u(0)\|)^T$. When $\|u(0)\|$ is small, well below 10^{-3}, the curves of Figure 2.2 match those of Figure 2.1, indicating that the evolution is essentially linear. For larger $\|u(0)\|$, larger than a threshold amplitude $\epsilon \approx 10^{-2}$, the nonlinearity has a pronounced effect, and the threshold amplitude is about 10^{-2}. Initial vectors larger than this do not decay to zero but blow up and are eventually attracted to a large-amplitude critical point of (2.2).

What is important about the behavior of Figure 2.2 is that the amplitude amplification exhibited is far greater than that of the purely linear problem. Table 2.1 lists the linear growth factor M and the threshold amplitude ϵ (for this particular initial vector) for four values of R. One sees that ϵ is of order M^{-2}, not M^{-1} as one might suppose from the idea that the growth mechanism is "only linear." This bootstrapping phenomenon can be explained as follows. Suppose the solution at time 0 consists of a vector of amplitude ϵ in the direction of the growing mode of (2.1). At later time the solution has grown to order $M\epsilon$ by the linear growth mechanism but moved into the decaying mode. Meanwhile, however, the nonlinear term in (2.2) has had the effect of transferring some of this energy back to the growing mode of (2.1), with amplitude $(M\epsilon)^2$ since the nonlinearity is quadratic. If $(M\epsilon)^2$ is of order less than ϵ, the process is not self-sustaining and energy dies away. On the other hand if $(M\epsilon)^2$ is of order greater than ϵ, then there is more energy than was present at the start and feedback occurs, leading to self-sustained amplitude growth and to an eventual amplitude, as it happens, on the order of R. Thus the threshold amplitude is $\epsilon = O(M^{-2})$.

Figure 2.3 gives another look at this model problem by depicting several trajectories in the phase plane $(u_1, u_2)^T$ for $R=5$. The linear term (A) forces trajectories to the right in the upper half-plane and to the left in the lower half-plane. For very small initial amplitudes the trajectories then turn a corner and head back to the stable critical point at the origin. The nonlinear term (B), however, superimposes on this linear portrait a counterclockwise rotation, transferring energy from the decaying to the growing mode of the linear term. For initial amplitudes larger than order R^{-2} the process is self-sustaining and the trajectory spirals up to the nonlinear critical point.

The growth process described here is "essentially linear" in the following respects. First, eq. (2.3) shows that the nonlinear term does not add energy to the system in a direct sense. (The same situation holds in hydrodynamics, as emphasized by Reddy and Henningson [RH].) Second, the growth process we have described is not specific to (2.3) but would apply to many different nonlinear terms. Any quadratic nonlinear term that transfers energy from decaying to growing modes is likely to generate a bootstrapping effect with threshold amplitude $\epsilon = O(M^{-2})$ much as in the experiment presented here. A random perturbation, for example, will often suffice. (Not *all* nonlinear terms are suitable; for example,

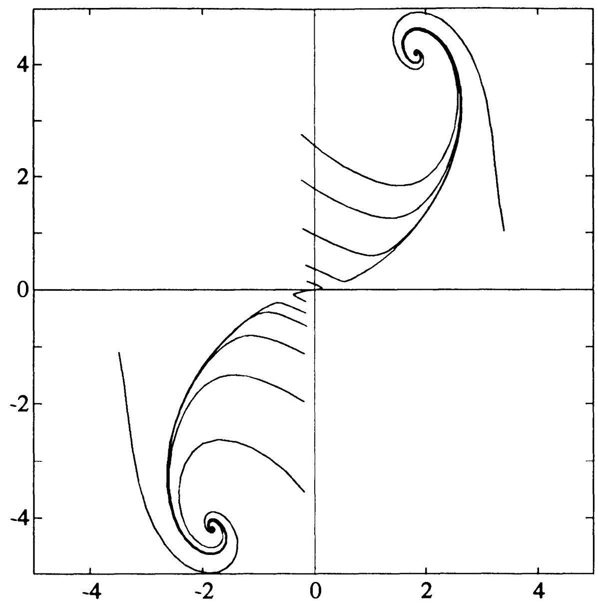

Figure 2.3. Trajectories in the phase plane for (2.2) with $R = 5$. The basin of attraction of the stable critical point at the origin is of width $O(R^{-2})$.

replacing B by its transpose transfers energy in the wrong direction.) Higher-order nonlinearities lead to similar effects, again independently of details; for example with a cubic nonlinear term one expects $\epsilon = O(M^{-3/2})$. Of course the critical points of the nonlinear system such as those of Figure 2.3 are entirely dependent on the nonlinear details, but that is the problem of turbulence, not instability. From amplitude $O(\epsilon)$ to $O(1)$ the nonlinear terms are small compared with the linear ones and the critical points are far away.

3. The linear Navier-Stokes evolution operator

Now we want to move from 2×2 matrices closer to fluid mechanics. Let $u_0 = u_0(x,y,z)$ be a time-independent solution to the Navier-Stokes equations in a geometry of interest. For plane Poiseuille and Couette flows the geometry is the infinite region bounded by two fixed plates at $y=0$ and $y=1$, and u_0 corresponds to the usual laminar flow solution between these boundaries—a parabolic velocity profile for Poiseuille flow, and a linear profile for Couette flow.

Let $u_0 + u(t) = u_0(x,y,z) + u(t,x,y,z)$ be a slightly perturbed solution to the Navier-Stokes equations. If we take u to be infinitesimal, then it satisfies an autonomous linear equation of the form

$$\frac{du}{dt} = -i\mathcal{L}u, \tag{3.1}$$

where $i = \sqrt{-1}$ and $\mathcal{L}$ is a linear operator. (The factor $-i$ is purely a matter of convention.) The precise choice of variables in the formulation of u is not essential to the idea of (3.1), but a convenient choice is to take u to be a vector consisting of the normal velocity and the normal vorticity, as described in [6], [BF] and [RH] ("normal" means in the y direction, normal to the solid boundaries). We will call the operator $\mathcal{L}$ the *linear Navier-Stokes evolution operator,* or the *Navier-Stokes operator* for short. The fundamental problem of linear stability theory is to analyze the evolution of solutions to this operator, or formally speaking, the operator exponential $e^{-it\mathcal{L}}$ [15,20]. In typical numerical calculations this translates to a matrix exponential for a matrix of dimension in the range 20–200.

The operator $\mathcal{L}$ is rarely mentioned in the literature of hydrodynamic stability. Instead, several reductions are made at the start of the discussion. First, one simplifies the problem by Fourier transforming in the unbounded variables x and z, introducing two real wavenumbers α and β, respectively. Second, one simplifies the problem further, in the Poiseuille case, by considering separately the evolution of even or odd perturbations (with respect to the centerline in y). Third, one assumes an exponential dependence with respect to t also, permitting a complex frequency ω.* It is in this step that the evolution problem (3.1) is replaced by an eigenvalue problem.

Because of Squire's theorem, a fourth simplification is also usually introduced, at least until the literature of the last few years. One sets $\beta = 0$, permitting only 2D perturbations.

The product of all four of these simplifications is the Orr-Sommerfeld equation: an eigenvalue equation in one spatial variable (y) in which the x wavenumber α appears as a parameter [2]. The analogous eigenvalue problem corresponding to 3D instead of 2D flow perturbations can be formulated in terms of coupled "Orr-Sommerfeld modes" and "Squire modes" [BF,RH], but seems to have no single

*Alternatively, one may take ω to be real and allow α to be complex. We do not consider this and other variations in this paper, but they are important.

name other than these. The 3D evolution problem (3.1), i.e., without eigenvalue analysis, seems to have no agreed-upon name at all, an indication of how prevalent the tendency in the hydrodynamic stability literature has been to equate linear analysis with eigenvalue analysis.*

The first two of these simplifications—Fourier transformation and even/odd separation—are physically reasonable, because the modes that are being separated are orthogonal. The situation is analogous to that of a block diagonal matrix, with the blocks corresponding to various choices of α, β, and even/odd; since the couplings between the blocks are zero, nothing is lost by analyzing them separately (at least for the linear problem). On the other hand the third simplification, looking at eigenvalues, is physically unreasonable when the eigenmodes are far from orthogonal, and this is analogous to the case of a triangular matrix in which the off-diagonal terms are far from zero. Though the off-diagonal terms in such a matrix have no effect on the eigenvalues, they may have a controlling effect on the actual behavior of the matrix in an evolution process [18].

The papers [BF] and [RH] are the first to analyze (3.1) systematically without making the physically unreasonable third and fourth steps just described. However, both of these papers do make the first and second simplifications involving α, β, and even or odd modes. Thus the spectra and pseudospectra that are discussed in those papers correspond to fixed choices of α, β, and even/odd. For example, Figure 5 of [RH] depicts the spectra and pseudospectra for Poiseuille flow with $\alpha=1$ and $\beta=0$ and $R=3000$. The spectrum takes the form of an asymmetric Y, a shape that has been familiar now for about 20 years [12,14]. Figure 7 of [RH] treats the same problem but with $\alpha=0$ and $\beta=2$, leading to a symmetric picture and a pure imaginary spectrum. This corresponds approximately to the "optimal" growth-maximizing mode of [BF], a streamwise vortex, which is now recognized as more important physically but is a less familiar picture.

The question with which we began this project was, what do the spectra and pseudospectra of the full operator $\mathcal{L}$ look like, i.e., with no restrictions at all? These sets are defined as follows:

$$\begin{aligned} \textbf{spectrum:} \quad \Lambda(\mathcal{L}) &= \{z \in \mathbb{C} : \|(zI-\mathcal{L})^{-1}\| = \infty\}, \\ \epsilon\textbf{-pseudospectrum:} \quad \Lambda_\epsilon(\mathcal{L}) &= \{z \in \mathbb{C} : \|(zI-\mathcal{L})^{-1}\| \ge \epsilon^{-1}\} \\ &= \{z \in \mathbb{C} : z \in \Lambda(\mathcal{L}+\mathcal{E}) \text{ for some } \mathcal{E} \text{ with } \|\mathcal{E}\| \le \epsilon\}. \end{aligned}$$

For a discussion of the idea of pseudospectra with computed matrix examples, see [18]; a comprehensive work is in preparation [19]. Because of the orthogonality described above, one has

$$\Lambda(\mathcal{L}) = \cup_{\alpha,\beta,\pm} \Lambda(\mathcal{L}_{\alpha,\beta,\pm}), \qquad \Lambda_\epsilon(\mathcal{L}) = \cup_{\alpha,\beta,\pm} \Lambda_\epsilon(\mathcal{L}_{\alpha,\beta,\pm}) \tag{3.2}$$

*See [8] for a discussion of an analogous situation in the literature of the numerical solution of ODEs.

where $\pm$ represents the even/odd choice in the Poiseuille case. Thus in principle, to find $\Lambda(\mathcal{L})$ or $\Lambda_\epsilon(\mathcal{L})$ one must look at the corresponding sets as computed by Reddy and Henningson or Butler and Farrell for all parameters α, β, $\pm$. In practice one performs a continuous optimization over α and β, once for the even modes and once for the odd modes. We have done this in Matlab on Sparc workstations, taking advantage of the codes of Reddy and Henningson based on Chebyshev spectral discretizations; we omit the details.

Unlike the spectrum, the pseudospectra $\Lambda(\mathcal{L})$ depend on the choice of norm $\|\cdot\|$.* For the results to be physically meaningful (and for (3.2) to be valid), one must pick a norm that corresponds to the square root of energy:

$$\text{Energy} = \|u\|^2. \tag{3.3}$$

If u consists of a velocity coupled with a vorticity, then the appropriate norm $\|\cdot\|$ is the weighted 2-norm obtained after a diagonal scaling of the vorticity terms by the wave number amplitudes; see [6], [RH], and [BF] for details.

In summary, the problem of optimal amplitude growth for the 3D linearized Navier-Stokes problem is the problem of the operator norms

$$\text{Amplitude: } \|e^{-it\mathcal{L}}\|$$

as a function of $t \geq 0$. For optimal energy growth we square this quantity and consider

$$\text{Energy: } \|e^{-it\mathcal{L}}\|^2.$$

*As must any quantity that is physically important.

4. Spectra and pseudospectra for plane Couette flow

Figures 4.1–4.4 depict the spectra and pseudospectra for Couette flows with $R = 250$, 500, 1000, and 2000. Note that the real and imaginary axes in these plots are not equally scaled. The various parts of these plots can be described as follows.

The shaded region in each plot is the spectrum $\Lambda(\mathcal{L})$. This was computed along the lines suggested in (3.2), by computing $\Lambda(\mathcal{L}_{\alpha,\beta})$ for values of α and β on a grid (there is no even/odd choice in the Couette case). The result is a set of dots in the complex plane that fill out a region that we take to be the spectrum and shade accordingly.

The three curves in each plot are the boundaries of the ϵ-pseudospectra $\Lambda_\epsilon(\mathcal{L})$ for $\epsilon = 10^{-2}$, $10^{-2.5}$, 10^{-3} (from upper to lower). These curves are obtained by computing $\|(zI - \mathcal{L})^{-1}\|$ at each point on a grid in the z-plane and then sending this grid data to a contour plotter. Each grid value requires an optimization over α and β, and thus these are large computations.

Finally, the asterisks along the imaginary axis represent the (discrete) eigenvalues for a case of particular interest: $\alpha = 0$ and $\beta = 1.6$, approximately the "optimal" mode of Butler and Farrell.

The plots in this and the next section are rough; so far, our data come primarily from Matlab computations with fairly small matrices. In particular, the boundary of the smallest ϵ-pseudospectrum in the plots is irregular in many cases, and sometimes appears to cut through the spectrum. This is impossible, and is an indication that our results are inaccurate. Such matters will be cleared up before final publication.

Let us consider what is revealed in Figures 4.1–4.4. First of all, the spectrum of $\mathcal{L}$ is always in the lower half-plane. This is well known, and corresponds to the fact that plane Couette flow is stable for all Reynolds numbers according to eigenvalue analysis.

The pseudospectra of $\mathcal{L}$, on the other hand, protrude far into the upper half-plane. If $\mathcal{L}$ were a normal operator, the boundary curve of $\Lambda_\epsilon(\mathcal{L})$ for each ϵ would lie exactly at a distance ϵ from $\Lambda(\mathcal{L})$. It is evident in the figures that the curves lie much further from $\mathcal{L}$ than this. In many respects, for a finite time at least, $\mathcal{L}$ will behave as if it has eigenvalues in the upper half-plane. In the later sections we will see what quantitative conclusions can be drawn from these pseudospectra.

One cannot see in Figures 4.1–4.4 what values of α and β correspond to various points in the spectrum and pseudospectra. We have not investigated this point in detail, but roughly speaking, the situation is as follows. The upper boundary of the spectrum corresponds to small values of β (less than 1) and values of α that grow in proportion to $\mathrm{Re}\, z$. The values of α in the pseudospectra are comparable, but the values of β are considerably larger. This is another reflection of the fact that although dominant eigenvalues can be taken to be two-dimensional, the non-modal aspects of this operator are strongly three-dimensional.

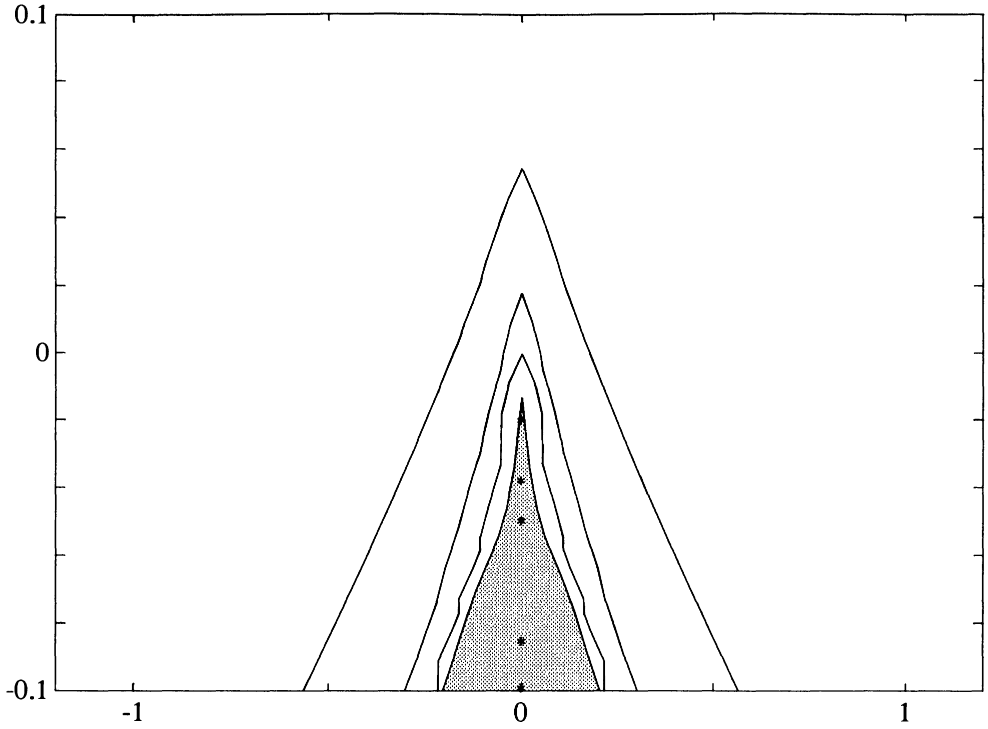

Figure 4.1. Spectrum (shaded) and ϵ-pseudospectra ($\epsilon = 10^{-2}$, $10^{-2.5}$, 10^{-3}) for Couette flow with $R = 250$.

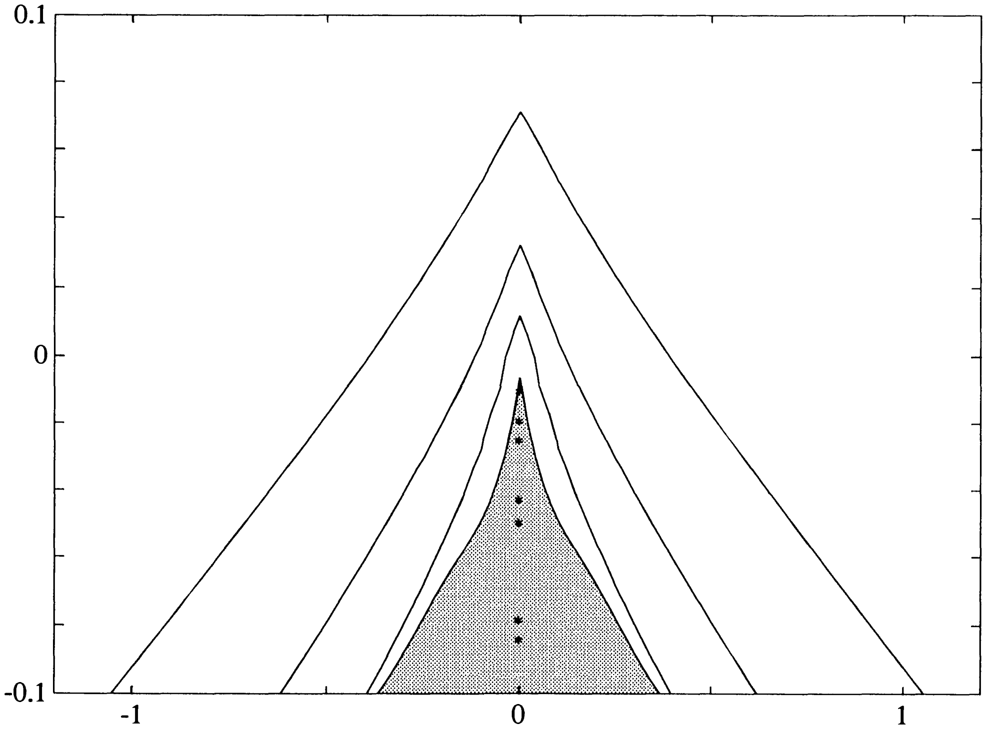

Figure 4.2. Couette flow, $R = 500$.

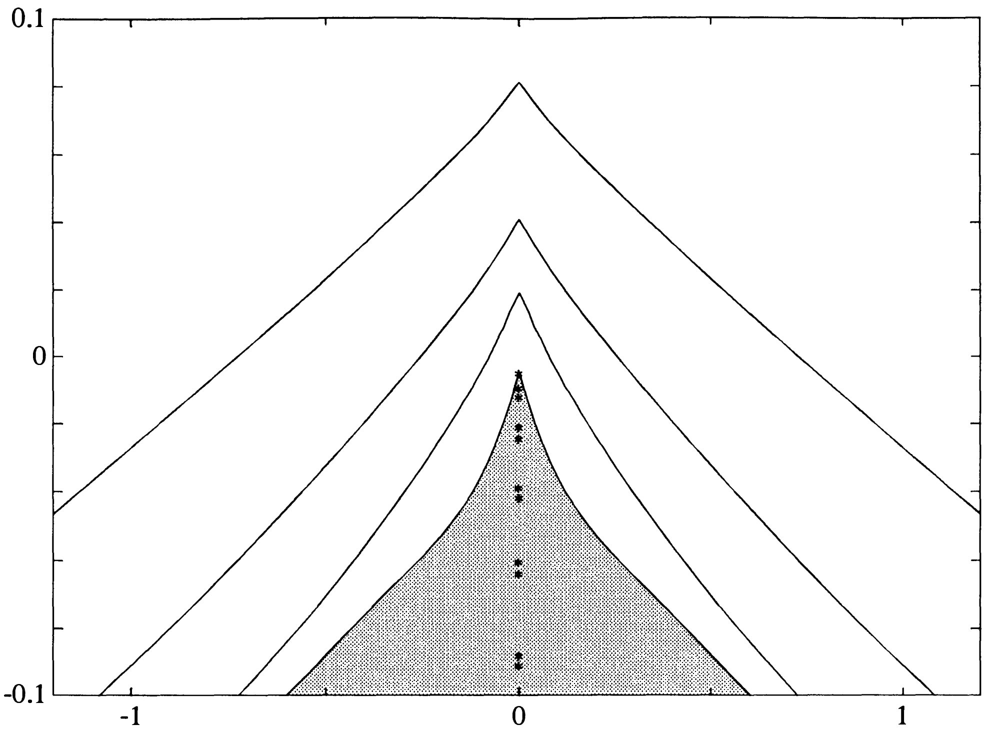

Figure 4.3. Couette flow, $R = 1000$.

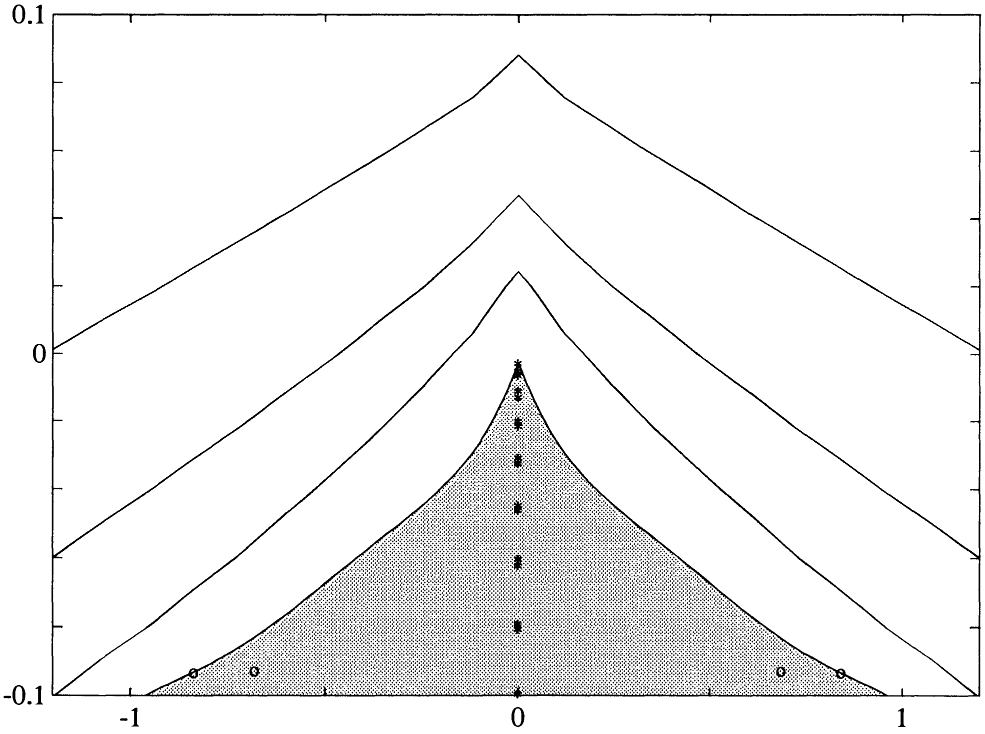

Figure 4.4. Couette flow, $R = 2000$.

5. Spectra and pseudospectra for plane Poiseuille flow

Figures 5.1–5.4 are analogous to Figures 4.1–4.4, but for Poiseuille instead of Couette flow. The Reynolds numbers are $R = 1000$, 3000, 5772, and 8000. The asterisks show eigenvalues corresponding to $\alpha = 1$ and $\beta = 2$, and the circles show eigenvalues corresponding to $\alpha = 0$ and $\beta = 0$ (the Y shape).

The geometry is more complicated here than in the Couette case. First of all there is the famous difference that in this case, for $R > 5772$, there is an eigenvalue in the upper half-plane. This dominant eigenvalue corresponds to the "mogul" that is visible in the four figures, which begins quite small at $= 1000$, becomes more prominent at $R = 3000$, hits the real axis at $R = 5772$, and then crosses into the upper half-plane for $R = 8000$. The modes that make up the mogul correspond to small values of $|\beta|$ (typically < 2) and values of α that grow approximately in proportion to $\mathrm{Re}\, z$. In particular, the most unstable point at the top of the mogul corresponds approximately to $\beta = 0$ (Squire's theorem) and $\alpha \approx 1$.

A second and quite distinct family of modes that delineates the spectrum is the "Mt. Fuji" branch, the steady slope that forms the boundary of the shaded region to the outside of the mogul and is continued as a dashed line underneath. This family corresponds to larger values of $|\beta|$, typically ≥ 2, and perturbations that are more highly three-dimensional.

The regions we have shaded are bounded by just these two families of eigenvalues, and represent a correct depiction of the spectrum $\Lambda(\mathcal{L})$ if attention is restricted to even modes. However, there is a further part of the spectrum corresponding to odd modes, also shaped like Mt. Fuji but with a higher imaginary part. This additional branch is marked by the highest of the dashed curves in our plots. Properly, this upper dashed curve should contribute to the boundary of the shaded region, but we have not yet carried out complete enough calculations for odd modes to draw this part of the picture properly. Hence our compromise: Figures 5.1–5.4 depict spectra and pseudospectra for even modes only, but the boundary of the odd mode spectrum is superimposed as an extra dashed line.

As in Couette flow, the pseudospectra tell a very different story from the spectra. The striking feature is that the mogul has negligible effect on the pseudospectra, indicating that it probably corresponds to modes at a substantial angle from the other eigenmodes of the system.* The action is in the pseudospectra, not the spectra, and near the imaginary axis, not near the mogul.

Fortunately, though these figures represent imperfectly the effects of odd modes near and below the uppermost dashed curve, the pseudospectral contours in the upper half-plane are probably correct for the full operator $\mathcal{L}$ with no restriction, for preliminary computations indicate that the even-mode resolvent norm is larger than the odd-mode resolvent norm in the upper half-plane.

*As mentioned in the last section, the cases where pseudospectral boundaries intersect the shaded region represent errors in our computations. So far as we know these are local errors, with little impact on the rest of the plot.

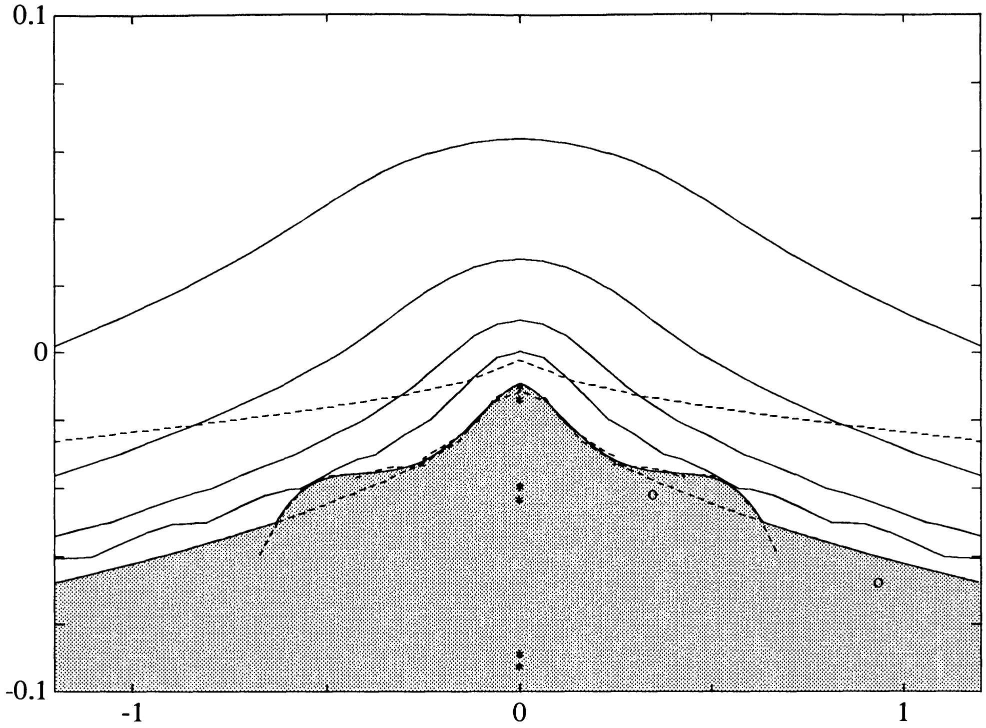

Figure 5.1. Spectrum (shaded) and ϵ-pseudospectra ($\epsilon = 10^{-2}$, $10^{-2.5}$, 10^{-3}, $10^{-3.5}$) for Poiseuille flow with $R = 1000$. See the text for comments about odd vs. even modes.

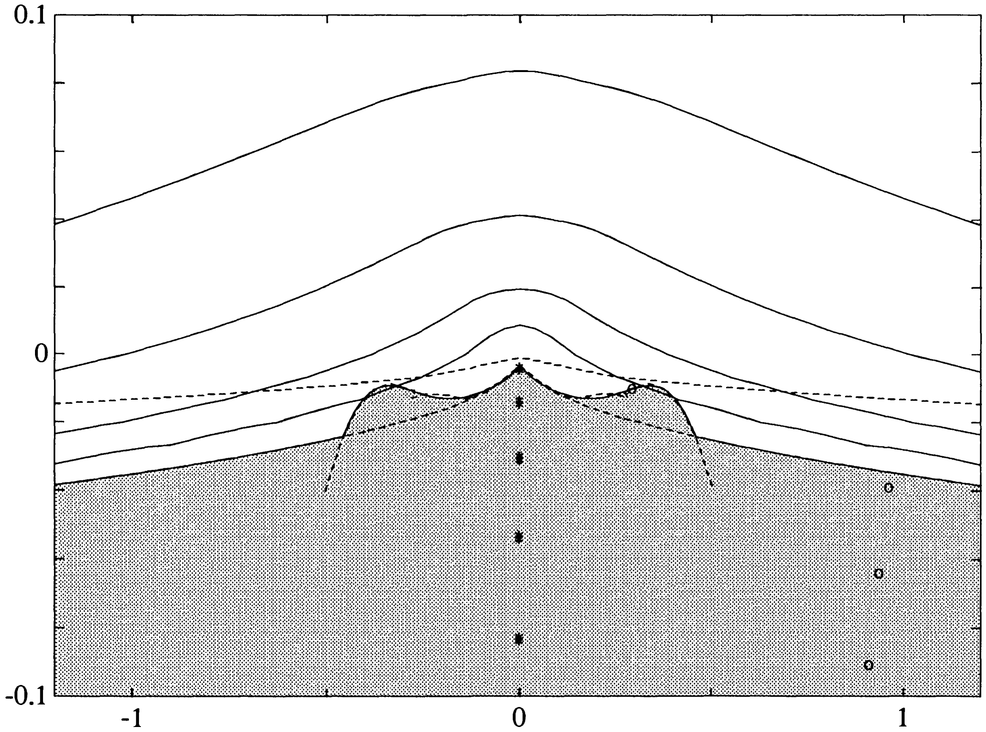

Figure 5.2. Poiseuille flow, $R = 3000$.

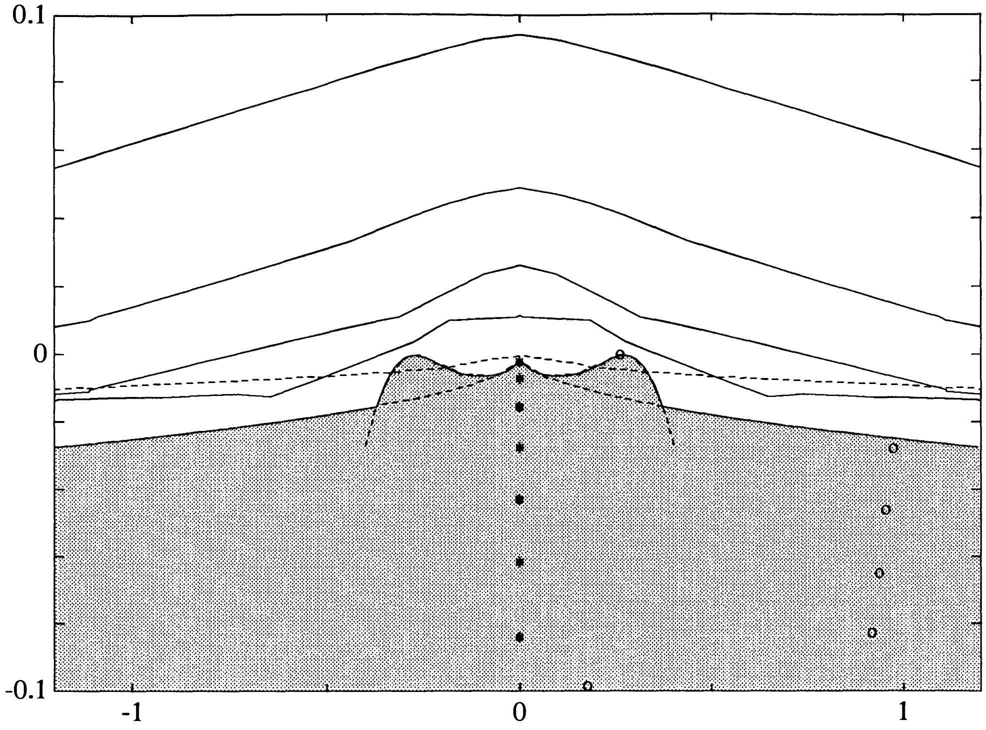

Figure 5.3. Poiseuille flow, $R = 5772$.

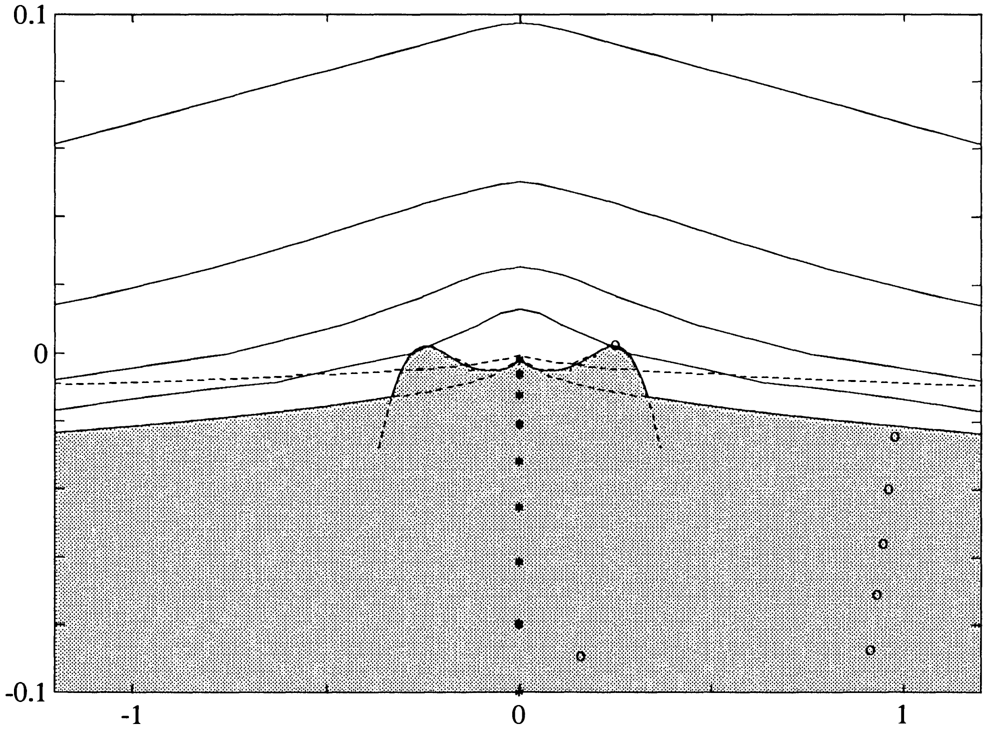

Figure 5.4. Poiseuille flow, $R = 8000$.

6. Transient energy growth estimates based on pseudospectra

The Butler-Farrell optimal perturbations are functions that achieve the maximum possible transient energy growth in a linear Navier-Stokes evolution process that has all its eigenvalues in the stable half-plane. It is interesting that by examining the pseudospectra of these operators in the unstable half-plane—without knowing anything about the problem they come from—one can predict that transient growth like this must occur and estimate its magnitude to within a factor of about 2. Bounds of this kind have been considered previously in [RH] and [14].

The estimate that makes this possible is a trivial one that might be called the "easy half of the Kreiss matrix theorem for exponentials" [11,13]. Suppose $\|e^{t\mathcal{L}}\| \le M$ for some constant M and all $t \ge 0$. Then by the Laplace transform, for any z with $\operatorname{Re} z > 0$ we have

$$\|(zI-\mathcal{L})^{-1}\| = \Big\|\int_0^\infty e^{-sz} e^{t\mathcal{L}}\, ds\Big\| \le M\Big|\int_0^\infty e^{-sz}\, ds\Big| = \frac{M}{|z|}.$$

Contrapositively, if $\|(zI-\mathcal{L})^{-1}\| \ge M/|z|$ for some M and some z with $\operatorname{Re} z > 0$, then we must have $\|e^{t\mathcal{L}}\| \ge M$ for some $t \ge 0$. Thus we have the bound

$$\sup_{t\ge 0} \|e^{t\mathcal{L}}\| \ge \sup_{\operatorname{Re} z>0} |z| \|(zI-\mathcal{L})^{-1}\|.$$

In particular, taking z to be a real number $y > 0$, and rotating by 90° in keeping with the usual convention of hydrodynamic stability gives

$$\sup_{t\ge 0} \|e^{-it\mathcal{L}}\| \ge \sup_{y>0} |y|\, \|(iyI-\mathcal{L})^{-1}\|. \tag{6.1}$$

We can state this bound in the language of pseudospectra if we define the ϵ-*pseudospectral abscissa* of $\mathcal{L}$ by

$$\sigma_\epsilon(\mathcal{L}) = \sup_{z\in\Lambda_\epsilon(\mathcal{L})} \operatorname{Im} z. \tag{6.2}$$

The estimate becomes

$$\sup_{t\ge 0} \|e^{-it\mathcal{L}}\| \ge \sup_{\epsilon>0} \frac{\sigma_\epsilon(\mathcal{L})}{\epsilon}. \tag{6.3}$$

From (6.3) and the pictures of the last two sections, with the aid of a ruler, one can estimate transient growth ratios. Consider for example Poiseuille flow with $R = 3000$. From Figure 5.2 one sees that the boundary of the ϵ-pseudospectrum with $\epsilon = 10^{-3.5}$ cuts the imaginary axis at a height of about 0.008. Thus we have $\sigma_{10^{-3.5}}(\mathcal{L}) \approx 0.008$ and therefore

$$\sup_{t\ge 0} \|e^{-it\mathcal{L}}\| \ge \frac{0.008}{10^{-3.5}} \approx 25.3,$$

or, squaring to measure energy,

$$\sup_{t\geq 0} \|e^{-it\mathcal{L}}\|^2 \geq 640.$$

The actual supremum in (6.3) for this problem is $29.3 \approx \sqrt{858}$ (determined with a computer instead of a ruler), attained with $\epsilon \approx 3.346 \times 10^{-5}$. Now the actual optimal growth for this problem is $42.0 \approx \sqrt{1763}$. Thus (6.3) falls short of the maximum by only about a factor of 2.

Tables 6.1 and 6.2 list the estimates (6.3) for a range of Reynolds numbers for both Poiseuille and Couette flow (compare Tables I, II, III of [BF]). The numbers reveal that in both the Poiseuille and Couette cases, the lower bound (6.3) captures about 70% of the optimal amplitude growth and thus about 50% of the optimal energy growth. Moreover, the wavenumber β that gives the optimal estimate (6.3) is virtually identical to the wavenumber of the true optimal. Clearly for this problem, the essential features of the growth mechanism are well represented in the pseudospectra of $\mathcal{L}$.

R	amplitude growth factor M	energy growth factor M^2	α	β
1000	9.78/14.0	95.6/196.	0/	2.05/2.05
3000	29.3/42.0	858./1763.	0/	2.05/
5000	48.73/69.98	2375./4898.	0/	/2.044
∞	$(R/102.6)/(R/71.45)$	$(R/102.6)^2/(R/71.45)^2$	0/0	/2.04

Table 6.1. Transient growth for Poiseuille flow at various Reynolds numbers. In each xx/yy pair, xx corresponds to the estimate (6.3) based on pseudospectra and yy to the actual Butler-Farrell optimal.

R	amplitude growth factor M	energy growth factor M^2	α	β
250	5.76/8.597	33.2/73.9	0/0.12	1.54/1.61
500	11.9/17.20	141.6/296.0	0/0.067	1.63/1.60
1000	23.5/34.42	552.3/1185.	0/0.035	1.63/1.60
2000	47.0/68.84	2211./4739.	0/0.018	1.62/1.60
∞	$(R/42.6)/(R/29.05)$	$(R/42.6)^2/(R/29.05)^2$	0/0	1.62/1.60

Table 6.2. Same as Table 6.1 but for Couette flow.

7. Minimal destabilizing perturbations

One method of coming to grips with the energy growth mechanism in linearized hydrodynamics is to study the Butler-Farrell "optimal," the initial function that achieves maximum possible transient energy growth before eventually decaying. In the language of linear algebra, this optimal is the dominant right singular vector for the operator $e^{t\mathcal{L}}$ with t chosen to maximize $\|e^{t\mathcal{L}}\|$ [5]. Another approach, considered in the last section, is to find the extremum of the pseudospectral estimate (6.3). This can be described as the dominant right singular vector for the operator $(iyI-\mathcal{L})^{-1}$ with y chosen to maximize $\|(iyI-\mathcal{L})^{-1}\|$. From the close agreement of the α and β parameters listed in Tables 6.1 and 6.2, it appears likely that both of these methods identify much the same streamwise vortex. We have not confirmed this in detail.

In this section we consider a third approach to understanding the destabilizing effects of non-normality. We ask: what is the minimal-norm perturbation $\mathcal{E}$ such that $\mathcal{L}+\mathcal{E}$ is unstable, i.e., has eigenvalues in the unstable half-plane? We call such an $\mathcal{E}$, or its norm, a *minimal destabilizing perturbation.* Equivalently, what is the smallest ϵ for which $\Lambda_\epsilon(\mathcal{L})$ touches the real axis? Also equivalently, what is the inverse of the largest value of $\|(zI-\mathcal{L})^{-1}\|$ for $z\in\mathbb{R}$?

From the pseudospectral plots of Sections 4 and 5 it is clear that the determining point in the complex plane is $z=0$ (except in Poiseuille flow with R greater than a number very slightly below 5772). Thus the question of minimal destabilizing perturbations reduces to the question, how large is $\|(zI-\mathcal{L})^{-1}\|$ for $z=0$? The corresponding function is the dominant right singular vector of $\mathcal{L}^{-1}$ itself, that is, the function that $\mathcal{L}$ most nearly annihilates. Questions like this of "nearness to instability" have received attention in the past decade in the literatures of numerical linear algebra and control theory. See for example [1], which contains a plot of a computed pseudospectrum, [9], and [10], where the minimal norm $\|\mathcal{E}\|$ is called the *stability radius* for $\mathcal{L}$. We are grateful to Ridgway Scott for suggesting that we apply these ideas to the Navier-Stokes operator.

The minimal destabilizing perturbation is a very different quantity from the the distance of the spectrum from the unstable half-plane. When a matrix or operator is non-normal, the minimal destabilizing perturbation may be far smaller than the location of the spectrum might suggest, and this turns out to be true for the Navier-Stokes problem. Tables 7.1 and 7.2 show that whereas the eigenvalue distance scales as R^{-1} (for $R<5772$, in the Poiseuille case), the minimal destabilizing perturbation scales as R^{-2}.

For Poiseuille flow with $R=1000$, for example, which is roughly the Reynolds number at which transition to turbulence is observed in the laboratory, Table 7.1 indicates that a perturbation $\mathcal{E}$ with $\|\mathcal{E}\|\approx 3\times 10^{-4}$ should be enough to make $\mathcal{L}+\mathcal{E}$ unstable. We emphasize that this is not a perturbation of the *data,* such as might be introduced by imperfections in the experimental apparatus, but a perturbation of the *operator.* The relevance of this to the evolution of fluid flow is that the

R	distance of spectrum from unstable half-plane	minimal destabilizing perturbation ϵ	α	β
500	4.93×10^{-3}	1.201×10^{-3}	0	1.62
1000	2.47×10^{-3}	3.010×10^{-4}	0	1.62
3000	8.22×10^{-3}	3.346×10^{-5}	0	1.62
5000	4.93×10^{-4}	1.205×10^{-5}	0	1.62
$\vdots$	$\vdots$	$\vdots$	$\vdots$	$\vdots$
∞	$(R/2.467)^{-1}$	$(R/17.36)^{-2}$	0	1.62

Table 7.1. Minimal destabilizing perturbations for Poiseuille flow at various Reynolds numbers. The last line represents convenient summary formulas; for $R > 5772$ in actuality a different eigenvalue from the one reflected here crosses into the upper half-plane.

R	distance of spectrum from unstable half-plane	minimal destabilizing perturbation ϵ	α	β
250	9.87×10^{-3}	1.051×10^{-3}	0	1.18
500	4.93×10^{-3}	2.633×10^{-4}	0	1.18
1000	2.47×10^{-3}	6.587×10^{-5}	0	1.18
2000	1.23×10^{-3}	1.647×10^{-5}	0	1.18
$\vdots$	$\vdots$	$\vdots$	$\vdots$	$\vdots$
∞	$(R/2.467)^{-1}$	$(R/8.117)^{-2}$	0	1.18

Table 7.2. Same as Table 7.1 but for Couette flow.

nonlinear terms can be thought of, locally, as introducing approximately such a perturbation, with the scale determined by the nature of the nonlinearities and the amplitude of the data (which in turn depends on those imperfections in the laboratory apparatus). We do not know if these ideas can be made precise enough to lead to a prediction of threshold amplitudes for transition to turbulence.

A comparison of the second columns of Tables 7.1 reveals that the distance of the spectrum from the upper half-plane is the same for Poiseuille and Couette flows (until R gets close to 5772 in the former case). The dominant eigenvalues that account for this in the Poiseuille case correspond to odd modes. If one restricts attention to even modes, the modes which dominate the pseudospectra in the upper half-plane, the distance of the spectrum changes to $(R/9.270)^{-1}$.

8. 3×3 and 4×4 approximations with 90% of the Butler-Farrell growth

The transient energy growth that is the subject of this paper and of [BF] and [RH] is not a phenomenon of individual eigenmodes. However, we have found that by projecting the linear Navier-Stokes operator $\mathcal{L}$ onto a 3-dimensional subspace in the Couette case, or a 4-dimensional subspace in the Poiseuille case, we can retain on the order of 90% of the energy growth of the full operator. In other words, much of the physics of transient energy growth can be captured by a 3×3 or 4×4 matrix, though not a 1×1 matrix.

The mechanics of such a projection are a matter of straightforward numerical linear algebra [5,14]. Having reduced $\mathcal{L}$ to an $N\times N$ matrix L by discretization, suppose we wish to project L onto the column space of an $N\times k$ matrix Q with orthonormal columns. The appropriate projected version of L is Q^*LQ. Suppose in particular that we started with an $N\times k$ matrix V whose columns are selected eigenvectors of L, satisfying $LV=VD$ for some $k\times k$ diagonal eigenvalue matrix D. If $V=QR$ is a QR (Gram-Schmidt) decomposition* of V, with Q of dimensions $N\times k$ and R of dimensions $k\times k$, then we have $Q^*V=R$ and $Q=VR^{-1}$ and therefore

$$Q^*LQ = Q^*LVR^{-1} = Q^*VDR^{-1} = RDR^{-1}. \qquad (8.1)$$

Thus RDR^{-1} (upper-triangular) is the matrix representation of the projection of L onto the space spanned by selected eigenvectors, and in Matlab its computation is a matter of a few lines.

The operator $\mathcal{L}$ and hence the matrix L are block 2×2 and block triangular; the diagonal blocks are the Orr-Sommerfeld and Squire operators described in [BF] and [RH]. It is convenient to label the various eigenvalues of $\mathcal{L}$ as OS or Squire eigenvalues, and number them by decreasing imaginary part. We have experimented with projections onto the spaces spanned by various subsets of the eigenmodes, and have reached the following conclusions. For Couette flow, most of the transient energy growth can be captured by projection onto a 3-dimensional subspace:

Couette: OS modes 1,3 and Squire mode 1.

For Poiseuille flow, most of the transient energy growth can be captured by projection onto any of three different 4-dimensional subspaces:

Poiseuille: OS mode 1 and Squire modes 1,2,3, or
OS modes 1,2 and Squire modes 1,2, or
OS modes 1,2,3 and Squire mode 1.

Figure 8.1 illustrates the Couette case for the fixed approximately optimal parameters $\alpha=0$, $\beta=1.6$. The solid curves are the norms $\|e^{t\mathcal{L}}\|$ as functions of t.

*Caution—we are using R for both the Reynolds number and a triangular matrix.

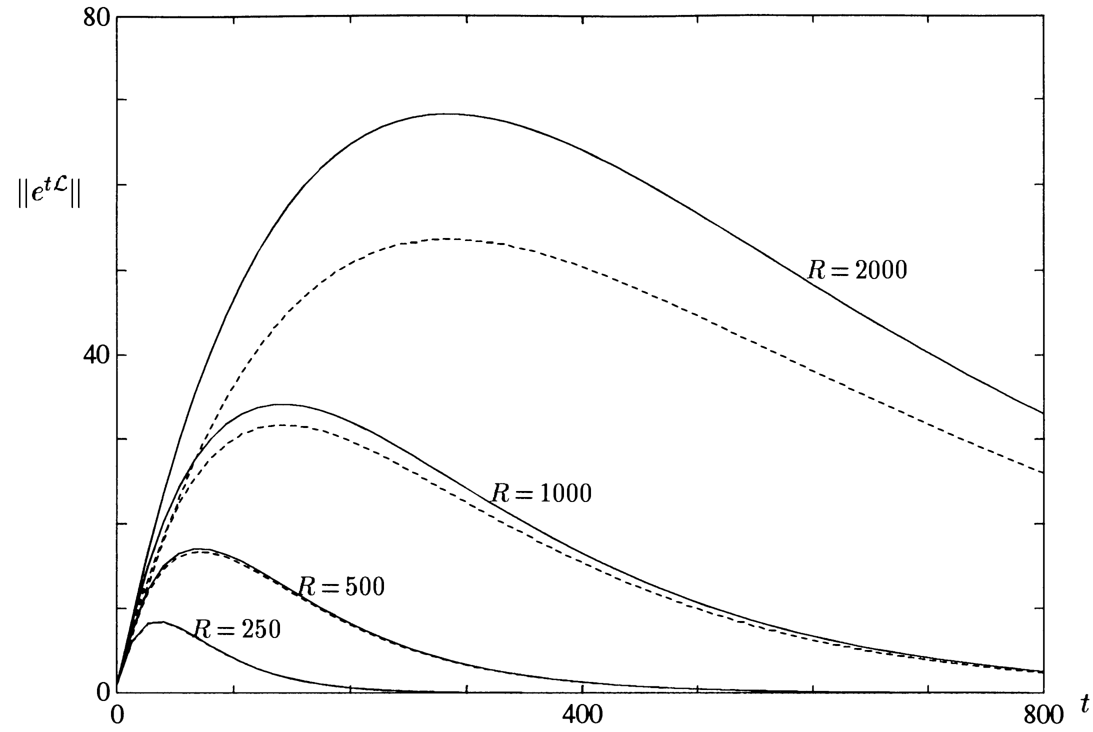

Figure 8.1. Transient amplitude growth for Couette flow (solid) and its 3×3 projection onto OS modes 1,3 and Squire mode 1 (dashed).

We plot amplitudes; for energies the numbers should be squared. The dashed curves are the corresponding norms after projection onto the space spanned by OS modes 1,3 and Squire mode 1.

Table 8.1 presents these results numerically, listing the fractions of the total amplitude and energies (squared amplitudes) obtained by these projections. For $R \leq 1000$ the 3×3 approximation evidently captures more than 86% of the energy growth.

R	amplitude	amplitude percentage	energy	energy percentage
250	8.416	99.24	70.82	98.49
500	16.58	97.88	274.9	95.80
1000	31.69	92.88	1004.	86.77
2000	53.76	78.69	2890.	61.92

Table 8.1. Percentage of the optimal amplitude and energy maxima achieved by the dashed curves of Figure 8.1 (Couette flow, $\alpha = 0$, $\beta = 1.6$).

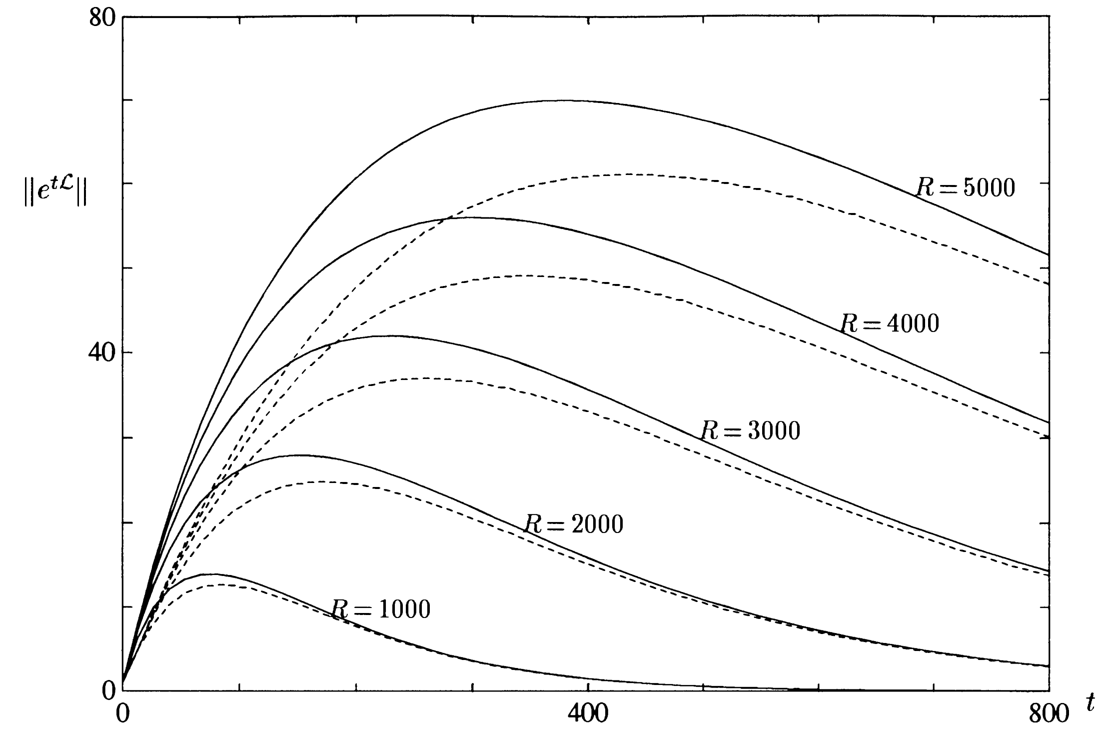

Figure 8.2. Transient amplitude growth for Poiseuille flow (solid) and its 4×4 projection onto 2 OS modes and 2 Squire modes (dashed).

Figure 8.2 and Table 8.2 are the the analogues of Figure 8.1 and Table 8.1 for a 4×4 approximation to the Poiseuille problem based on 2 OS modes and 2 Squire modes, with $\alpha = 0$ and $\beta = 2.04$. As in the Couette case, the low-dimensional approximation is obviously a good one, capturing more than 76% of the total energy growth for the Reynolds numbers shown.

R	amplitude	amplitude percentage	energy	energy percentage
1000	12.75	91.17	162.7	83.13
2000	24.85	88.87	617.4	78.98
3000	37.02	88.20	1370.	77.79
4000	49.11	87.72	2411.	76.94
5000	61.13	87.35	3737.	76.30

Table 8.2. Percentage of the optimal amplitude and energy maxima achieved by the dashed curves of Figure 8.2 (Poiseuille flow, $\alpha = 0$, $\beta = 2.04$).

It is interesting to examine, for this Poiseuille problem, what combinations of modes suffice to capture a substantial fraction of the energy growth of the full operator $\mathcal{L}$ (still with $\alpha=0$, $\beta=2.04$). Table 8.3 lists results for various numbers of OS and Squire modes, for $R=5000$:

no. of OS modes	no. of Squire modes	amplitude percentage	energy percentage
1	1	8.09	0.69
2	2	87.35	76.30
3	3	97.61	95.27
4	4	99.40	98.81
1	2	50.86	25.87
1	3	88.80	78.85
1	4	94.40	89.11
1	5	95.07	90.37
2	1	43.55	18.97
3	1	85.10	72.43
4	1	94.93	90.11
5	1	96.35	92.84
2	3	89.16	79.49
3	2	88.30	77.96

Table 8.3. Dependence of transient growth on the choice of eigenmodes included in the low-dimensional approximation (Poiseuille flow, $R=5000$, $\alpha=0$, $\beta=2.04$).

The numbers in this table are closely related to the recent results of Gustavsson [6]. For a slightly different choice of α and β, Gustavsson showed that a huge amount of transient energy growth can be achieved by a model consisting of one OS mode and many Squire modes. The independent results of [BF] then showed that Gustavsson's model had captured about 90% of the optimal energy growth, a conclusion that is reproduced in the figures above. The figures show that the combination of one OS mode with many Squire modes is not the only one that works; one can do just as well, for example, by taking 1 Squire mode and many OS modes.

Here are some 3×3 matrices for Couette flow. For $R=500$:

$$A = i\times\begin{pmatrix} -0.01005 & 0.16652 & -0.62491 \\ 0 & -0.01896 & -0.11473 \\ 0 & 0 & -0.04953 \end{pmatrix}. \tag{8.2}$$

For $R=1000$:

$$A = i\times\begin{pmatrix} -0.00503 & 0.08533 & -0.60812 \\ 0 & -0.00948 & -0.10894 \\ 0 & 0 & -0.02477 \end{pmatrix}. \tag{8.3}$$

The scaling of these matrices as a function of R appears to be

$$A = R^{-1} \begin{pmatrix} O(1) & O(1) & O(R) \\ & O(1) & O(R) \\ & & O(1) \end{pmatrix}, \tag{8.4}$$

which is not far from the 2×2 model of Section 2.

9. The 3×3 model with nonlinearity

In Section 2 we presented a 2×2 model problem in which a locally energy-conserving nonlinear term had the effect of bootstrapping a linear growth mechanism into a nonlinear instability. In the last section we showed that although this 2×2 matrix does not seem to arise in the equations of linearized hydrodynamics, analogous matrices do seem to arise, to good approximation, of dimensions 3×3 and 4×4. To conclude this paper we will now close the loop by illustrating that the bootstrapping effect applies also to these more realistically obtained matrices. In particular we consider the 3×3 matrix corresponding to Couette flow with $R = 1000$.

In analogy to (2.2), consider

$$u_t = Au + \|u\|^\nu Bu, \qquad B = \begin{pmatrix} 0 & 1 & 1 \\ -1 & 0 & 1 \\ -1 & -1 & 0 \end{pmatrix} \tag{9.1}$$

with A defined by (8.3). The parameter ν is 1 for a quadratic nonlinearity, 2 for a cubic nonlinearity, and so on. Figures 9.1 and 9.2 are analogues of Figures 2.2 with $\nu = 1$ and $\nu = 2$, respectively, based on initial vectors of the form $u(0) = (0, 0, \|u(0)\|)^T$. Clearly the behavior is much the same as in Figure 2.2. Below a threshold initial amplitude, the evolution is approximately linear. Above that amplitude, there is positive feedback and eventual growth to a large-amplitude critical point.

The observed threshold amplitudes are

$$\nu = 1: \quad \epsilon \approx 2.3 \times 10^{-6},$$

$$\nu = 2: \quad \epsilon \approx 2.5 \times 10^{-4}.$$

Both of these numbers are far less than the inverse of 31.69, the linear growth factor listed in Table 8.1. For threshold energies instead of amplitudes, we square these numbers and find ourselves at the level of 10^{-8} or below.

The next step in this analysis should be to replace the arbitrary nonlinear term in (9.1) by some approximation to the actual nonlinear terms present in the Navier-Stokes equations [7]. These terms transfer energy not only between modes for fixed α and β, but also across modes (see e.g. [7]). One could then attempt to estimate threshold perturbation amplitudes for transition to turbulence in a fashion that would be quantitative rather than merely suggestive.

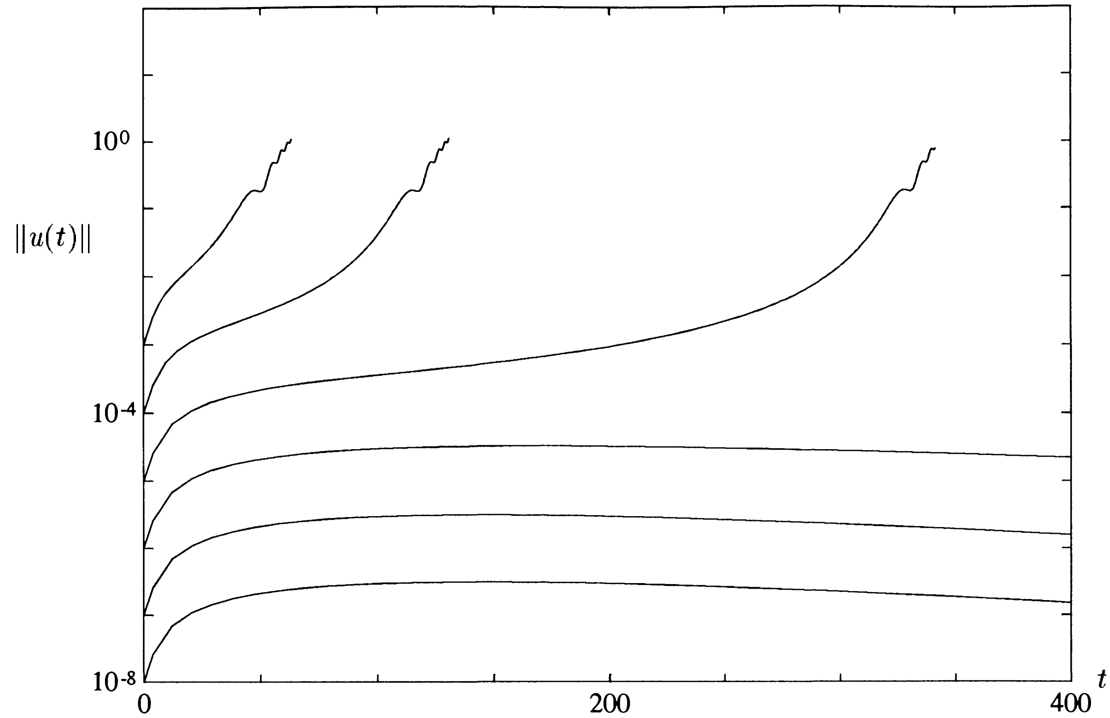

Figure 9.1. $\|u(t)\|$ vs t for solutions to the model problem (9.1) with quadratic nonlinearity ($\nu=1$). Compare Figure 2.2. The threshold amplitude is $\epsilon \approx 2.3 \times 10^{-6}$.

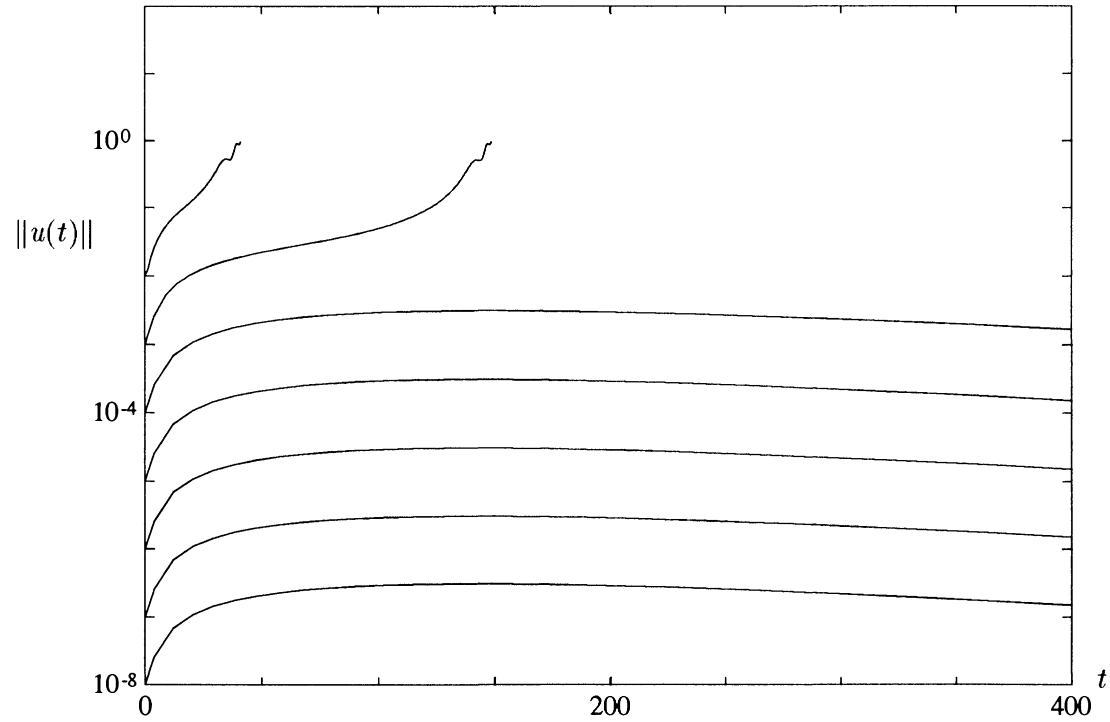

Figure 9.2. Same as Figure 9.1 but for a cubic nonlinearity ($\nu=2$). The threshold amplitude is $\epsilon \approx 2.5 \times 10^{-4}$.

Acknowledgments

This paper would not have been written without the continuing advice over several years of Dan Henningson. We have also benefited from "non-modal" discussions with Peter Schmid, Brian Farrell, and Kathryn Butler, and from discussions on various topics with Walter Mascarenhas, Philip Holmes, Ridgway Scott, and André Weideman. Finally, our computations have been made possible by a remarkable software system, Matlab.

References

[BF] K. M. Butler and B. F. Farrell, *Three-dimensional optimal perturbations in viscous shear flows,* Phys. Fluids, to appear.

[RH] S. C. Reddy and D. S. Henningson, *Energy growth in viscous channel flows,* J. Fluid Mech., submitted.

---

[1] J. W. Demmel, *A counterexample for two conjectures about stability,* IEEE Trans. Aut. Control AC-32 (1987), 340–342.

[2] P. G. Drazin and W. H. Reid, *Hydrodynamic Stability,* Cambridge U. Press, Cambridge, 1981.

[3] B. Farrell, *The initial growth of disturbances in a baroclinic flow,* J. Atmos. Sci. 39 (1982), 1663–1686.

[4] B. F. Farrell, *Optimal excitation of perturbations in viscous shear flow,* Phys. Fluids 31 (1988), 2093–2102.

[5] G. H. Golub and C. F. Van Loan, *Matrix Computations,* 2nd ed., Johns Hopkins University Press, Baltimore, 1989.

[6] L. H. Gustavsson, *Energy growth of three-dimensional disturbances in plane Poiseuille flow,* J. Fluid Mech. 224 (1991), 241–260.

[7] D. S. Henningson and P. J. Schmid, *Vector eigenfunction expansions for plane channel flows,* Stud. Appl. Math., to appear.

[8] D. J. Higham and L. N. Trefethen, *Stiffness of ODEs,* BIT, to appear.

[9] N. J. Higham, *Matrix nearness problems and applications,* in M. J. C. Gover and S. Barnett, eds., Applications of Matrix Theory, Oxford U. Press, 1989, pp. 1–27.

[10] D. Hinrichsen and A. J. Pritchard, Real and complex stability radii: a survey, in D. Hinrichsen and B. Mørtensson, eds., Proc. Workshop Control of Uncertain Systems, Birkhäuser, 1989, pp. 119–162.

[11] R. J. LeVeque and L. N. Trefethen, *On the resolvent condition in the Kreiss matrix theorem,* BIT 24 (1984), 584–491.

[12] S. A. Orszag, *Accurate solution of the Orr-Sommerfeld stability equation,* J. Fluid Mech. 50 (1971), 689–703.

[13] A. Pazy, *Semigroups of Linear Operators and Applications to Partial Differential Equations,* Springer-Verlag, Berlin, 1983.

[14] S. C. Reddy, P. J. Schmid, and D. S. Henningson, *Pseudospectra of the Orr-Sommerfeld operator,* SIAM J. Appl. Math., to appear.

[15] D. H. Sattinger, *The mathematical problem of hydrodynamic stability,* J. Math. Mech. 19 (1970), 797–817.

[16] P. J. Schmid and D. S. Henningson, *A new mechanism for rapid transition involving a pair of oblique waves,* Phys. Fluids, to appear.

[17] M. N. Spijker, *On a conjecture by LeVeque and Trefethen related to the Kreiss matrix theorem,* BIT 31 (1991), 551–555.

[18] L. N. Trefethen, *Pseudospectra of matrices,* in D. F. Griffiths and G. A. Watson, Numerical Analysis 1991, Longman, 1992.

[19] L. N. Trefethen, *Spectra and Pseudospectra: The Behavior of Non-Normal Matrices and Operators,* book to appear.

[20] V. I. Yudovich, *The Linearization Method in Hydrodynamical Stability Theory,* Amer. Math. Soc., Providence, 1989.